Bull. Astr. Soc. India (2011) **39**, 409–428

Black hole transients

T. M. Belloni,[1*] S. E. Motta[1,2] and T. Muñoz-Darias[3,1]

[1]*INAF– Osservatorio Astronomico di Brera, Via E. Bianchi 46, I-23807 Merate, Italy*

[2]*Università dell'Insubria, Via Valleggio 11, I-22100 Como, Italy*

[3]*Instituto de Astrofísica de Canarias, Calle Vía Láctea s/n, 38205 La Laguna, Tenerife, Spain*

Received 2011 August 23; accepted 2011 September 12

Abstract. Sixteen years of observations of black hole transients with the Rossi X-ray Timing Explorer, complemented by other X-ray observatories and ground-based optical/infrared/radio telescopes have given us a clear view of the complex phenomenology associated with their bright outbursts. This has led to the definition of a small number of spectral/timing states which are separated by marked transitions in observables. The association of these states and their transitions to changes in the radio emission from relativistic radio jets completes the picture and have led to the study of the connection between accretion and ejection. A good number of fundamental questions are still unanswered, but the existing picture provides a good framework on which to base theoretical studies. We discuss the current observational standpoint, with emphasis onto the spectral and timing evolution during outbursts, as well as the prospects for future missions such as ASTROSAT (2012) and LOFT (>2020 if selected).

Keywords : accretion, accretion discs – black hole physics – X-rays: binaries

1. Introduction

The first black hole transient (BHT), A 0620−00, was discovered more than thirty years ago (Elvis et al. 1975) and already showed that the spectral evolution of these objects was very complex. The first major step forward came with the Japanese satellite Ginga, which thanks to the presence of an all-sky monitor and a large pointed detector led to the discovery and detailed study of a few objects (Tanaka & Lewin 1995). Complex variability patterns were discovered, including Quasi-Periodic Oscillations, which led to the extension of the hard/soft states of black hole binaries (originally developed for Cygnus X-1) to additional states (see e.g., Miyamoto et al. 1993). Because of the scarcity of sources and of coverage, Ginga data gave only a limited view of

*email: tomaso.belloni@brera.inaf.it

the spectral/timing evolution of BHTs. Around the same epoch, optical observations yielded the first strong dynamical evidence for a BH (i.e. compact object heavier than $\sim$3 $M_\odot$) in A 0620−00 (McClintock & Remillard 1986), which was fully confirmed a few years later by Casares et al. (1992) with the measurement of a mass function >6 $M_\odot$ in another BHT, the Ginga source GS 2023+338 (=V404 Cyg). The situation changed with the launch of the Rossi X-ray Timing Explorer (RXTE) at the end of 1995. Sixteen years of operations (with high level of flexibility and fast response) led to the observation of a large number of objects through extensive campaigns, often with coordinated observations at other wavelengths (see e.g., Remillard & McClintock 2006). From this wealth of data, clear patterns emerged which are now leading to the development of theoretical models. The evolution of spectral, timing and spectral/timing parameters can now be classified into a small number of states which can be easily identified and followed throughout an outburst (see Belloni 2010), as well as linked to observations at lower energies (see Fender 2010). In this paper, we summarize the current observational status, focussing on the outburst evolution and spectral states, and briefly discuss the contributions from upcoming missions like ASTROSAT and LOFT.

2. The tools of the trade: fundamental diagrams

The behaviour of BHTs is known to be easily characterized in terms of spectral states and transitions between them. These states, dubbed "canonical" by Miyamoto et al. (1992), are defined on the basis of the spectral and timing properties displayed by the sources during their outburst phases (see Sec. 3). The canonical states become apparent in a hardness–intensity diagram (HID), where the total count rate is plotted as a function of the spectral hardness (defined as the ratio of observed counts in two energy bands). Here the spectral evolution of many BHTs can be followed along a q-shaped pattern that is traced anti-clockwise. In the HID (see Fig. 1, top-left panel) four different branches can be identified, corresponding to the four sides of the "q" (the fact that the transition from hard to soft takes place at higher flux than the reverse transition is seen in all systems, see Maccarone & Coppi 2003). The right and left vertical branches respectively match the low hard state and the high soft state already known before the RXTE era. In between these two well-established states, the situation is rather complex and the intermediate points that fill this region roughly correspond to those previously know as very-high state and intermediate state. These two states show very similar properties in the spectral domain, making it practically impossible to distinguish between them (see Homan et al. 2001). However, when the timing properties are taken into account, the "intermediate region" of the HID can be easily divided into two well separated areas, as they show completely different features in the time-domain (see Sec. 3). It is important to remark that not all transients show a regular evolution like the one which will be described here. However, the basic states and their properties can be defined for all systems. For an overview of a large number of RXTE transients see Dunn et al. (2010).

The first step towards a clear distinction of the intermediate regions is made by looking at the hardness–rms diagram (HRD, see Fig. 1, bottom-left panel), where the fractional rms, integrated over a broad range of frequencies, is plotted versus hardness. In this diagram, unlike in the HID, most of the points follow a correlation over a single line (no hysteresis here), extended from the

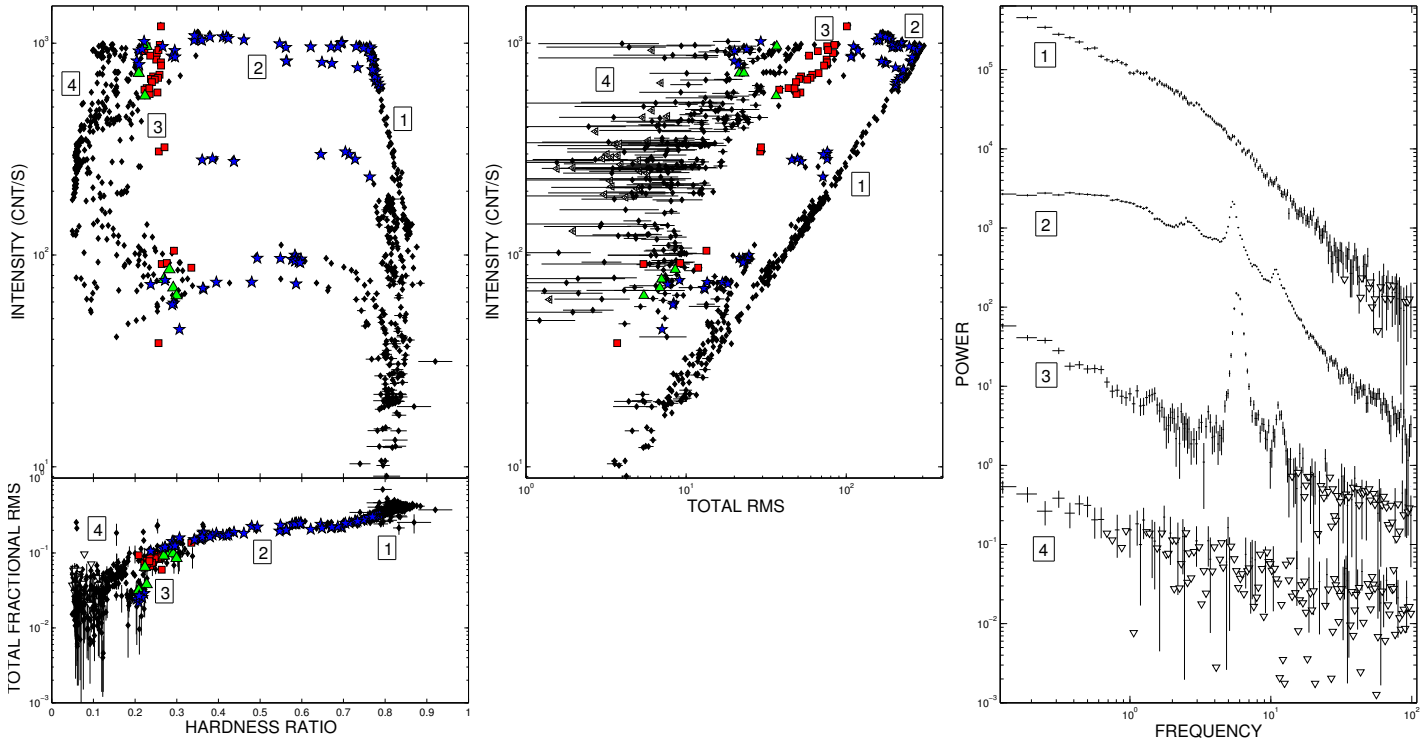

Figure 1. Top-left panel: HID for the 2002, 2004, 2007 and 2010 outbursts of GX 339–4, with each point representing a single RXTE observation. Bottom-left panel: the corresponding rms-hardness diagram, with empty triangles representing upper limits. The hardness ratio is defined as the ratio of net counts in the 6.1−20 keV band over those in the 3.3−6.1 keV band. Middle panel: RID for the 2002, 2004, 2007 and 2010 outbursts of GX 339–4. Symbols are as follows. Blue stars: Type-C QPOs; red squares: Type-B QPOs; green triangles: Type-A QPOs; black dots: all the other RXTE observations of GX 339–4 that do not show low-frequency QPOs. Right panel: Power density spectra for the four regions marked in the left and middle panels. The left and middle panels have been adapted from Motta et al. (2011).

softest points, where the points show a low level of variability (<5%), to the hardest points, where the variability is much higher (also exceeding 30%). In the region at intermediate hardness, the correlation is rather tight; however in a narrow hardness ratio band several points show a lower variability than the points on the main correlation (see Fig. 1). This behaviour already suggests the presence of two separate states in this region, corresponding to the points on the main correlation (spanning a very large range in hardness and rms) and to those deviating from it (found in a narrow hardness and rms range). However, it is only by examining the fast aperiodic variability that the canonical states can be distinguished clearly from one another.

Examining the Power Density Spectra (PDS) allows one to probe the fast timing properties of a source. It is worth mentioning that although important information can be extracted from higher-order timing tools (such as phase/time lags, coherence and bicoherence, see Nowak & Vaughan 1996; Maccarone & Schnittman 2005), these are not essential for the basic determination of states and state transitions. A number of different PDS shapes can be observed in BHTs, but it is now clear that we can classify them as belonging to a few basic types that are closely related to the position on the HID and HRD (in addition there are a few more complex PDS shapes, not shown here, associated to the "anomalous" state found at very high accretion rate in some sources, Belloni 2010). The most prominent features in the PDS are narrow peaks, known as low frequency quasi periodic oscillations (QPOs). QPOs have been discovered in many systems and, even though their physical origin is still under debate (see Motta et al. 2011, and references therein), they are thought to originate in the innermost regions of the accretion flows around stellar-mass black holes.

Low-frequency QPOs (LFQPOs) with frequencies ranging from a few mHz to ~20 Hz were already found in several sources with Ginga and divided into different classes (see e.g., Miyamoto et al. 1993; Takizawa et al. 1997). Observations performed with the RXTE have led to an extraordinary progress in our knowledge on properties of the variability in BHBs and it was only after RXTE was launched that LFQPOs were detected in most observed BHBs (see van der Klis 2006; Remillard & McClintock 2006; Belloni 2010, for recent reviews). Three main types of LFQPOs, dubbed types A, B, and C, originally identified in the PDS of XTE J1550–564 (see Wijnands et al. 1999; Homan et al. 2001; Remillard et al. 2002), have been seen and identified in several sources. All the basic types of PDS (with the exception of the additional ones related to the "anomalous" state) were observed in the outbursts of GX 339–4 between 2002 and 2011(see Fig. 1, right panel).

- The hard points in the HID (region [1] in Fig. 1, left-upper panel) show a PDS similar to [1] in Fig. 1 (right panel). Its shape can be fitted with a small number of very broad Lorentzian components. In some cases also a low-frequency QPO peak is observable at very low frequencies ($\nu \leq 0.01$ Hz). The characteristic frequencies (see Belloni et al. 2002) of all these components increase with source flux, while the energy spectrum (see below) softens gradually.

- PDS [2] in Fig. 1 can be considered a high-frequency extension of PDS [1]. It is found at intermediate hardness values (region [2] in Fig. 1, top-left panel). The most promi-

nent feature is a QPO with centroid frequency varying between ∼0.01 and ∼20 Hz and a quality factor Q around 10. The characteristic frequencies of all Lorentzian components vary together, including that of the QPO. As in the previous case, they are correlated with hardness: softer spectra correspond to higher frequencies and also to lower integrated rms variability (see Fig. 1, middle panel). The LFQPO observed here is termed "type-C" QPO (stars in Fig. 1, see Casella et al. 2005; Motta et al. 2011, for a precise definition of the three QPO types) and it always appears together with moderately strong (10–30% rms) band-limited noise. It is often accompanied by two peaks harmonically related: one at half the frequency and one at twice the frequency, with the higher one having a similar Q to that of the fundamental; higher harmonics are often observed (Rao et al. 2010). The frequency of the type-C QPO is strongly correlated with the characteristic (break) frequency of the main underlying broad-band noise components (see Wijnands & van der Klis 1999; Belloni et al. 2002), a correlation which also extends to neutron-star binaries.

- Over a narrow range of intermediate hardness, PDS similar to region [3] in Fig. 1 can be found (region [3] in the HID, see Fig. 1, top-left panel). These PDS feature a QPO called "type-B" (squares in Fig. 1). This oscillation shows different properties from type-C QPOs. The fact that type-B QPOs are not simply an evolution of type-C QPOs is demonstrated by the fast transitions observed between them (see Takizawa et al. 1997; Nespoli et al. 2003; Casella et al. 2004; Belloni et al. 2005). Type-B QPOs are associated with a weak power-law noise that replaces the broad Lorentzian components of the previous PDS types. Type-B QPOs show a harmonic structure similar to that of type-C QPOs (harmonic peaks and a peak at 1/2 the frequency of the main peak). While type-C QPOs span large range in frequency, type-B QPOs are limited to the range 1–6 Hz, but detections during high-flux intervals are concentrated in the narrow 4–6 Hz range (see Motta et al. 2011). The centroid frequency appears positively correlated with source intensity rather than hardness.

- At hardness values systematically slightly lower than those of PDS [3], PDS showing "type-A" QPO can be observed (triangles in Fig. 1). Being a much weaker and broader feature, we know less details about this oscillation. Sometimes it is only detected by averaging observations. Its frequency is always in the very narrow range 6–8 Hz and it is associated to an even lower level of power-law noise than type-B.

- The three types of QPOs can be separated by plotting them against the integrated fractional rms of the PDS in which they appear (see Casella et al. 2005; Muñoz-Darias et al. 2011a; Motta et al. 2011).

- The softest points in the HID (region [4] in Fig. 1, left panels) show PDS ([4] in Fig. 1, right panel) with a weak steep component, which often needs a long integration time for a detection. Weak QPOs at frequencies higher than 10 Hz are sometimes observed, as well as a steepening/break at high frequencies. The total fractional rms can be as low as 1%.

- In addition to the PDS shapes described, there are two types of PDS which are not always observed in BHTs. One PDS has a featureless curved shape, the other with additional broad and narrow features (see e.g., Belloni 2010).

By the introduction of a third fundamental diagram, the rms-Intensity diagram (RID, see Muñoz-Darias et al. 2011a), it becomes possible to clearly separate the canonical states without the intervention of any spectral information. To produce the HID and the RHD three variables are needed: spectral hardness, intensity (or count rate) and integrated fractional rms. The RID is the third possible plot between these variables: the integrated rms (not fractional) as a function of the total count rate. In the RID, the fast variability can be used as a good tracer of different accretion regimes in black hole binaries and it becomes apparent that apart from the linear rms-flux relation (a.k.a. hard line) found during LHS (see Gleissner et al. 2004), different relations are followed during the soft and intermediate states, to the extent that it is possible to identify the states from the RID alone. State transitions produce marked changes in the rms-flux relation. It is also important to notice that, in the RID, type-B QPOs (that are the defining feature of the SIMS, see Sec. 3) appear in a well-defined region between 5 and 10% fractional rms. This fact virtually removes the necessity of a detailed analysis of the PDS to separate the intermediate states (see Sec. 3). A detailed description of the RID and its properties and peculiarities can be found in Muñoz-Darias et al. (2011a).

It is important to remark that the diagrams described above are instrument dependent and source dependent, which means that a quantitative comparison between them is not always possible. However, they are also model independent and provide very precise measurements. For a discussion of similar diagrams based on spectral fits, see Dunn et al. (2010).

3. Timing-spectral states

The diagrams presented in the previous section lead to the definition of small number of states, whose boundaries are rather precise and defined by the data (see also Homan & Belloni 2005; Belloni et al. 2006; Belloni 2010). It is important to stress that it is possible to characterize these states only by considering both spectral and timing properties, so that the concept of "spectral" states carries little meaning. While the states do not have direct physical connection, their definition is a necessary step in order not to miss major physical changes in the accretion flow.

- **The Low-Hard State (LHS)**. Only (and possibly always, but there are quite a few cases of missed starting LHS) at the beginning and at the end of an outburst. It corresponds to the right nearly-vertical branch in the HID (the spectrum softens as the flux increases). The energy spectrum is hard and usually associated to thermal Comptonization (Gilfanov 2010). Strong (> 30% fractional rms) variability in the form of a band-limited noise is present (see PDS [1] in Fig. 1, right panel). As flux increases, the total fractional variability in most cases decreases. At high rates, the end of this state is marked by the leaving of the hard line (see Fig. 1, middle panel), while the actual shape of the power density spectrum changes more gradually across the transition.
- **The Hard-Intermediate State (HIMS)**. It corresponds to horizontal branches in the HID. It takes place after the initial LHS and before the final LHS, as well as in the central parts of the outburst, through mini state transitions. The energy spectrum is softer than in the

LHS and at low hardness an accretion disc component starts contributing to the RXTE/PCA band. The variability is dominated by a weaker band-limited noise and a type-C QPO (stars in Fig. 1, left and middle panels, PDS [2], right panel; for a discussion of the different types of QPO see Casella et al. 2005; Motta et al. 2011). The fractional rms decreases with hardness down to ∼10%; overall, the evolution of the power spectra is such that they are an extension of the LHS ones. The QPO frequency is anti-correlated with hardness and correlated with the photon index of the hard spectral component.

- **The Soft-Intermediate State (SIMS)**. When both hardness and fractional rms drop below well defined thresholds (0.71 for GX 339–4, see Fig. 1), the source enter the SIMS. Here the energy spectrum is similar to that of the nearby HIMS (at least below ∼ 10 keV, see below), but the timing properties are completely different: the band-limited noise disappears (drop in the HRD, rms below 10%) and is replaced by a power-law noise, while a marked type-B QPO is present (squares in Fig. 1, PDS [3]), whose frequency correlates with the hard X-ray flux (see Motta et al. 2011).

- **The High-Soft State (HSS)**. The leftmost branch in the HID. Here the spectrum is soft, dominated by a thermal disc contribution. A hard component is observed with varying intensity. Very little variability is observed (PDS [4] in Fig. 1, right panel), sometimes with type-A QPOs. This state spans a larger range in luminosity.

The main time evolution of a transient are: LHS – HIMS – SIMS - HSS as accretion rate increases, followed by HSS – SIMS – HIMS – LHS as accretion rate decreases (for a discussion of the reverse transition from soft to hard see Kalemci et al. 2006; Belloni et al. 2006). Intermediate minor transitions between states, usually not involving the LHS, can be observed. In some sources the initial LHS (or LHS – HIMS) is so fast that it is not observed. Some sources never leave the LHS, in very few cases reaching the HIMS without showing a transition to the SIMS (Capitanio et al. 2009; Motta et al. 2010). Very few sources show a more complex time evolution, which however involves observations that can be classified in one of the four states outlined above. In addition, an "anomalous state" is present in some sources, related to very high luminosities (see Belloni 2010; Done & Kubota 2006). The level at which the LHS – HIMS transition takes place can vary in one source from outburst to outburst, but it is always higher than the reverse transition and their level appear to be anti-correlated: a brighter upper HIMS branch corresponds to a fainter lower HIMS branch (see Maccarone 2003; Dunn et al. 2010). What physical quantity determines the flux (and accretion rate) level at which the hard to soft transition takes place is currently unknown, although it has been suggested that the time from the previous outburst plays a role (Yu & Yan 2009, and references therein).

4. Energy spectra

Timing properties are crucial to define the states, but although few models have been proposed to explain the origin and the nature of time-variability, still there is not a clear interpretation nor an explanation on their physical origin.

Even though we are still far from achieving a clear and complete comprehension of the full accretion mechanism acting in X-ray binaries, we have an idea of the main physical processes involved. Here we will discuss spectral variations along the HID and we will mainly focus on the changes that take places during spectral transitions. Note that the information we discuss in this section is mainly based on the 2–200 keV energy band since a good portion of it comes from RXTE data. Very detailed spectra come from instruments with higher spectral resolution.

The emission coming from X-ray binaries cover a very broad energy interval, extending from the radio to the very high energies (hard X-rays and sometimes gamma-rays). The main effects of the accretion mechanism in the region close to the compact object can be observed in the X-rays, but other fundamental processes are responsible for the emission at very different wavelengths (see also Sec. 7). The X-rays consist of both thermal emission coming from the very inner regions of an optically thick accretion disc as well as a harder component, extending to hundreds of keV and sometimes up to an MeV. The characteristics of this hard component are state-dependent. In the hard states (LHS and HIMS), it is usually interpreted as thermal or hybrid Compton radiation from the interaction of the soft disc photons with relativistic electrons in the inner regions of the accretion flow (see Done et al. 2007; Gilfanov 2010, for recent reviews). It has also been suggested that non-thermal Comptonization processes (e.g., self-Compton from synchrotron emission from the jet or bulk motion Comptonization) could be responsible for this component (Laurent & Titarchuk 2001; Markoff 2010). For the soft states (HIMS and HSS), the hard component extends to higher energies and is possibly of non-thermal origin.

The movement of a source along the HID must be decomposed in vertical (i.e. count rate) and horizontal (i.e. spectral hardness) excursions. The vertical movement, typical of the hard state where the spectrum softens less dramatically, is thought to be driven by accretion rate, depending on the geometry of the system and of the accretion flow. The horizontal movement is caused by a combination of a steepening of the hard component and the appearance of a thermal disc component in the RXTE band. While accretion rate most likely continues increasing, the marked change in accretion properties is triggered by a hitherto unknown parameter (but see Yu & Yan 2009).

- **LHS** ([1] in Fig. 1) – as already mentioned, all outbursts most likely start in this state, although at times it is not observed, probably because of its short time scale. The corresponding broad-band energy spectra are very hard and usually show a high-energy cutoff around 50–100 keV (spectrum 1 in Fig. 2). In GX 339–4 and GRO J1655–40 this cutoff was seen to move to lower energies as flux increased (see Fig. 3), together with a steepening of the photon index. A faint cold disc with a large inner radius and a peak temperature of few tenths of keV is sometimes observable if the interstellar absorption is low (see e.g., Muñoz-Darias et al. 2010). However, in few sources a hot thermal disc has been detected, suggesting that in some cases the inner disc radius could be always close to the innermost stable orbit. Sometimes an additional non-thermal component is also present in the spectrum (Markoff et al. 2002). This component has been proposed to be associated with the synchrotron jet detected at radio waves.

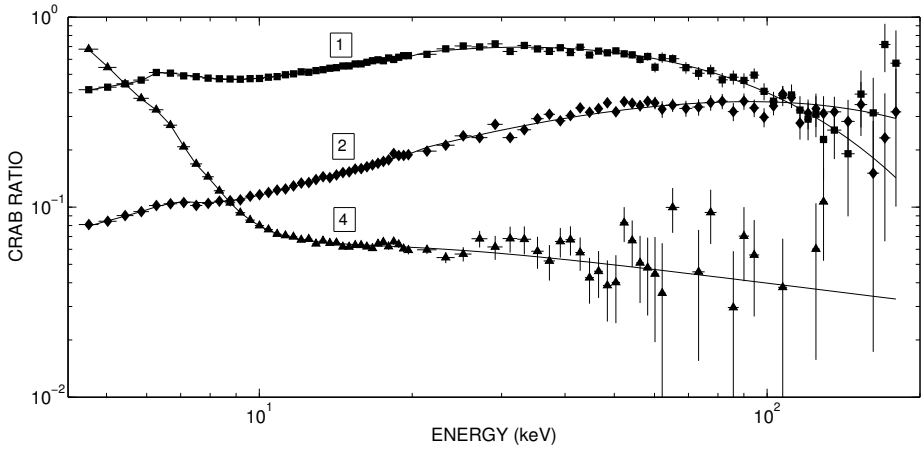

Figure 2. PHA ratio of GX 339–4 to Crab for three selected observations. (1) LHS spectrum, (2) HIMS spectrum, (4) HSS spectrum. Figure adapted from Motta et al. (2009).

- **HSS** ([4] in Fig. 1) – the energy spectrum is dominated by the thermal emission from the disc, observed with a small inner disc radius and a temperature that reaches typical values of ∼1 keV. The hard component, probably the result of Comptonization of soft photons on a non-thermal distribution of relativistic electrons, is in general very faint and variable without an observed cutoff below 1 MeV (spectrum 4 in Fig. 2).

- **HIMS/SIMS** ([2] and [3] in Fig. 1) – during the HIMS and the SIMS, the transition from hard to soft state takes place. The spectrum is a combination of the soft and hard component dominating the HSS and LHS respectively (spectrum 2 in Fig. 2). In several sources the inner disk radius has been observed to move inward during these states. This behaviour provides a physical explanation to the changes in the spectral shape during the transition, partially produced by the increasing soft emission coming from the disc. Whether the cutoff decreases, increases or disappears in the intermediate states has been a topic of debate for several years. This has been partially solved thanks to the good coverage achieved for some sources. In GX 339–4 (Motta et al. 2009, see Fig. 3) and GRO J1655–40 (Joinet et al. 2008), after the decrease during the LHS, the high-energy cutoff is observed to suddenly increase in the HIMS, to reach its maximum in the SIMS. If a high energy cutoff is present in the HSS, it is not observable below 1 MeV (Del Santo et al. 2008). The decrease seen during the LHS is thought to be produced by the cooling of the Comptonizing medium due to the higher fraction of soft photons undergoing Comptonization, while the reason for the HIMS increase is still under discussion. Spectra from the softest HIMS and from the SIMS are very similar, since their hardness is very similar and the evolution from one to the other is smooth (for a discussion, see Stiele et al. 2011).

As mentioned above, some sources (e.g., GRO 1655–40) display another state, the "anom-

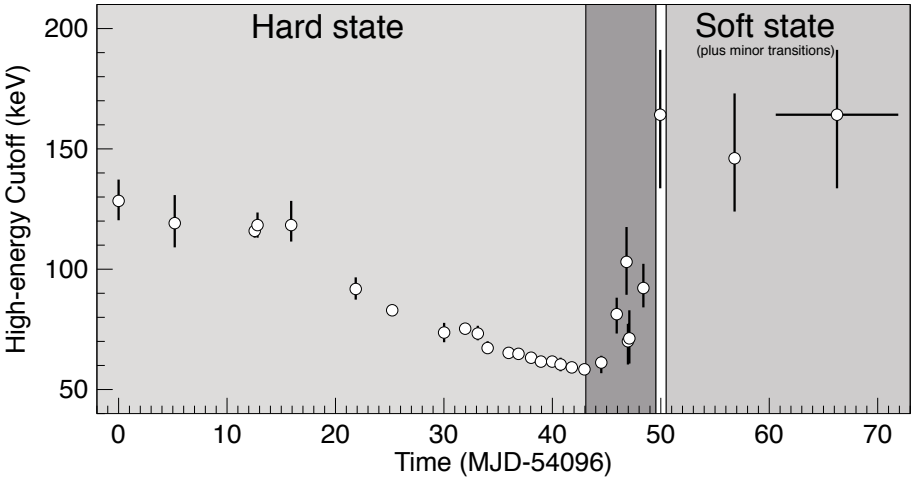

Figure 3. Evolution of the high-energy cutoff in the 2007 outburst of the BHT GX 339–4.

alous" or "ultra-luminous" state. Here, the source shows very high luminosities and the energy spectrum appears dominated by a soft disc component. The disc component allows to infer a high inner-disc temperature associated to a small inner disc radius, while the hard component is steep and faint.

5. Rms spectra

The amount of variability as a function of energy is another observable which is seen to vary along the outburst. This is expected, since the relative contribution of each spectral component strongly depends on the accretion state. Apart from its average spectral shape, usually measured over long time scales ($\geq$ 1 ks), each component also prompts a certain level of variability in the observed light-curve. The shape of the rms spectrum (i.e., fractional rms as a function of energy) encodes information directly related to the relative contribution of each emission process and the intrinsic origin of the variability itself. Whereas the former can also be obtained from spectral studies, the latter results in unique insights into accretion physics.

As for many other cases, the RXTE/PCA has made a strong contribution, most of the results present in the literature being referred to the $\sim$ 2–20 keV energy band. In a first approximation, rms spectra with three different shapes are observed in BHT: flat, rms decreasing with energy (soft; aka., inverted) and increasing with energy (hard). The first two cases correspond to the hard states (see below), whereas a hard rms spectrum is seen as the system softens. In Fig. 4 we show an example of these shapes using RXTE/PCA data of GX 339-4 during its hard-to-soft transition.

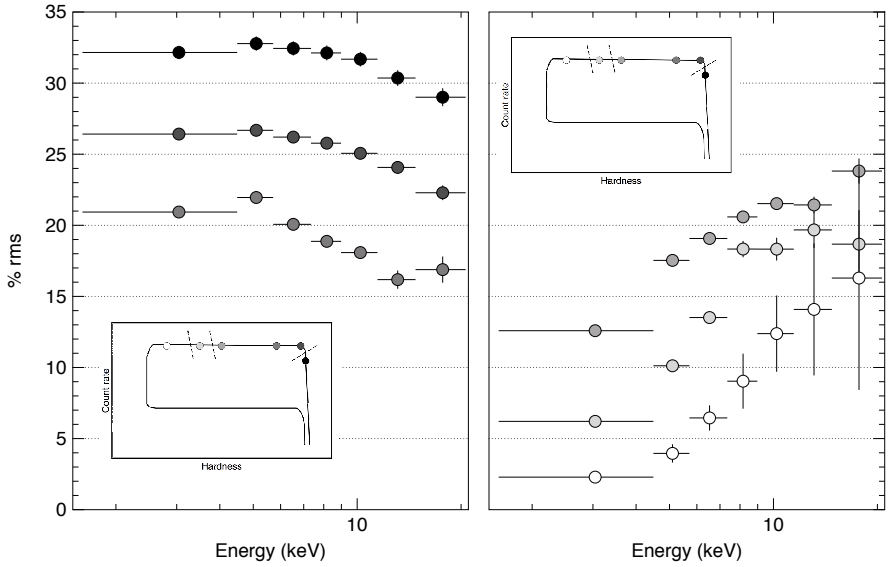

Figure 4. Evolution of the 0.1–32 Hz rms spectrum along the hard-to-soft transition of GX 339–4. Left panel, from top to bottom: rms spectra from a bright LHS, a hard HIMS and a softer HIMS (see inset). Right panel, from top to bottom: rms spectra from a HIMS just before the transition, a SIMS and a HSS (see inset).

- **LHS**: Flat and inverted rms spectra are observed during this state. Clear examples of the former are e.g., XTE J1550–564 (Gierliński & Zdziarski 2005), Cyg X–1 or XTE 1752–223 (Muñoz-Darias et al. 2010). The latter behaviour is observed in XTE J1650–500 (Gierliński & Zdziarski 2005) or Swift 1753.5–0127 (Soleri et al., submitted). Flat rms spectra are easily explained by considering that variability arises from variations in the normalization of one single spectral component. This could account for what we see in the hard state, where the hard component is dominant ($\geq$ 2 keV; see Sect. 4). Variations in the spectral shape of this component (i.e., not only in normalization) need to be taken into account to explain inverted rms spectra. Gierliński & Zdziarski (2005) (see also Zdziarski et al. 2002) show that a strongly varying (disc) seed photon input can produce inverted rms spectra, since it varies the spectral shape by making the power-law to pivot around $\sim$ 50 keV. Variations in the normalization of the power-law component are also needed to reproduce the observed dependence of the rms with energy. Interestingly, in some of the cases where flat rms spectra are observed, they are still consistent with being inverted at $\sim$ 1–2% level (e.g., Fig. 4).

- **HIMS:** As it happens for several spectral and timing parameters, a major change in the shape of the rms spectra is observed along the HIMS. Whereas LHS-like rms spectra are observed during the early stages of the HIMS, they harden as the system approaches the soft states. This transition occurs fast; for instance, the two last HIMS spectra presented in Fig. 4 are separated by five days. Their corresponding energy spectra are different as

well, since the disc component is only present in the second one. Muñoz-Darias et al. (2011a) observed a flux increase at constant absolute variability in correspondence to the appearance of the disc component in the energy spectra of this system during the HIMS. The above suggests disc variability to be low at least during last (softest) stages of the HIMS.

- **SIMS and HSS:** Hard rms spectra are observed during soft states. As shown in Fig. 4, these are remarkably similar to those observed at the softest end of the HIMS, but with total variability decreasing as the system softens. These patterns can be explained by considering no or very little disc variability, which results in lower rms values in the soft band when disc dominates. Above 5–10 keV, where the variable power-law dominates, we recover the flat shape observed in the LHS.

5.1 The origin of the variability and the role of the disc component

It has been known for years that variability is mainly associated with the hard component rather than the disc. During soft states, where the disc dominates, low variability levels ($\leq$ 5 per cent) are observed. Even there, its energy dependence also points to a hard-component origin (see e.g., Gilfanov 2010 and references therein). HIMS observations also point in the same direction (see above) and in the LHS, where only the hard component is present above $\sim$ 2 keV, we see the highest variability levels. Paradoxically, Comptonization models aiming at explaining the inverted rms spectra require a highly variable disc during the LHS. Softer ($\leq$ 2 keV) XMM observations have shed some light on this issue. Evidence for low frequency ($\lesssim$1 Hz) disc variability during the LHS has been reported by Wilkinson & Uttley (2009). Also at low frequencies, Uttley et al. (2011) published time-lag measurements showing disc variability leading hard-component variability. Both results represent a strong evidence for a variable disc component during the LHS at low frequencies (Gierliński & Zdziarski 2005), whereas for time scales shorter than $\sim$ 1 s (i.e. those typically used for variability studies) results are not conclusive.

If variability originates in the soft component, it should progressively disappear to explain the lack of variability observed as the energy spectrum softens. Hard-component variability should decrease as well, but high levels of hard-component variability are observed during soft states. Interestingly, Muñoz-Darias et al. (2011b) report a dramatic fade of hard-component variability during the SIMS in MAXI J1659–152. The light curve associated to the disc component is also shown to be more stable at very low frequencies once the system reaches the HSS.

We note that the role played by the jet component, which is probably highly variable (e.g., Casella et al. 2010) and has been proposed to account in some cases for the observed X-ray emission during the LHS (e.g., Markoff et al. 2001) should be much better understood to solve this problem. The combination of multiwavelength studies and the broader spectral coverage planned for future X-ray missions, such as LOFT (Feroci et al. 2011) and ASTROSAT (Agrawal 2006), should make a decisive contribution to this issue.

6. High-frequency oscillations

Despite the large number of available RXTE observations of black hole binaries, only a handful of detections of quasi-periodic peaks above 30 Hz is available (see Belloni et al. 2006, and references therein). Three sources show a single QPO peak, although for two of them the detection is not very significant and in the case of XTE J1650–500 the peak appears only after stacking spectra from a specific state. Four other sources show two peaks, which when detected more than once appear at almost the same frequency: GRO J1655–40 (300 and 450 Hz), XTE J1550–564 (184 and 276 Hz), H 1743–322 (165 and 241 Hz) and GRS 1915+105 (41 and 69 Hz). In the first three cases, the frequencies are consistent with being in 3:2 ratio, for GRS 1915+105 the ratio is 5:3. Interestingly, an additional peak at 27 Hz was found in GRS 1915+105, which is in 2:3 ratio with 41 Hz (Belloni et al. 2001). These features are very important as they constitute the highest-frequency signals from accreting black holes and they are most likely related to effects of General Relativity in the strong field regime. This is not the place to discuss more details or applicability of models, but it is important to remark that all these detections correspond to sources in (or close to) the SIMS. The case of GRS 1915+105 is more complex, as the association of its features with the four states described above is not simple (see Reig, Belloni & van der Klis 2003; Soleri, Belloni & Casella 2008).

7. The multi-wavelength view

The phenomenology described above was found to have strong links with the properties of relativistic jets as observed in the infrared and radio bands. The radio emission offers the possibility to study the synchrotron emission related to the relativistic jets (see Fender 2010; Gallo 2010), while in the IR, optical and UV bands the thermal emission from the companion star and from the outer edge of the disc can be observed (see e.g., Homan et al. 2005; Russell et al. 2006; Migliari et al. 2007).

The basic properties are summarized in Fig. 5. In the LHS, a steady compact jet is observed, with a flat or inverted spectrum and a barely resolved spatial distribution. The radio and infrared fluxes are correlated with the X-ray flux, correlation which extends to the AGN when the proper mass scaling is considered (see Coriat et al. 2011, and references therein). The infrared flux also correlates with the X-ray one.

At the top of the LHS branch, in GX 339–4 the correlation between X-ray and infrared was observed to break down (Homan et al. 2005). As the source follows the HIMS and approaches the transition to the SIMS, the radio spectrum starts steepening (Fender et al. 2004). Around, but not exactly at the time of the transition (Fender et al. 2009), a radio flare is observed (or the ejection time of a fast relativistic resolved jet). The hardness threshold at which this happens has been dubbed "jet line". After the source enters the HSS, no nuclear radio emission has been detected up to know, as all detections are compatible with emission from the ejecta. Recent observations of 4U 1957+11 have put the limit to more than 300 times lower than the LHS radio flux at the same X-ray flux (Russell et al. 2011).

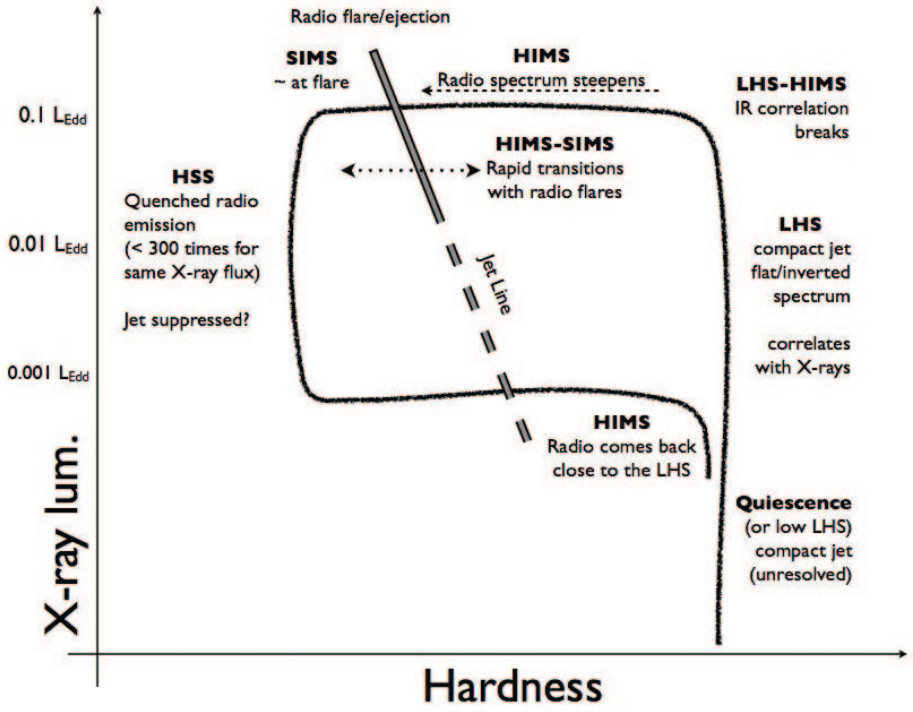

Figure 5. Stylized hardness-intensity diagram for a BHT with labels indicating the radio properties.

In correspondence of additional transitions back and forth between HIMS and SIMS, there is some evidence that more radio flares are emitted in XTE J1859+226, (see Brocksopp et al. 2002), and in GRS 1915+105 where the oscillations have been connected to such transitions (Fender & Belloni 2004).

On the return transition, the radio emission becomes detectable again, but at a higher hardness value than it disappeared earlier, when the source has already reached the LHS (Kalemci et al. 2006). The radio/X-ray correlation is re-established and can be followed down to very low accretion rate (Gallo et al. 2006).

7.1 Optical and infrared timing

The advent of new instrumentation during the last decade (e.g., ULTRACAM; Dhillon et al. 2007) has enabled us to extend some of the timing studies, classically performed at high energies, to the optical and infrared domains with unprecedented quality. In contrast to what is typically observed in neutron stars (e.g., Muñoz-Darias et al. 2007), complex cross correlation functions, with optical variability leading and anti-correlated to X-rays were found in BHT during the LHS

(e.g., Kanbach et al. 2001; Durant et al. 2008). These features cannot be explained solely by reprocessing on the accretion disc (see Hynes et al. 2003) and theoretical interpretations proposed generally require of a substantial contribution to the optical emission from the synchrotron jet observed at radio waves (Malzac et al. 2004; but see Veledina et al. 2011). This interpretation is also supported by some spectral energy distribution studies, which point to a significant jet contribution to the OIR (optical-infrared) and maybe to higher energies during the LHS (e.g., Markoff et al. 2001; Russell et al. 2010) and by high time resolution studies performed in the near IR (Casella et al. 2010). To gauge the jet contribution to the OIR is an important open issue since it has strong implications in, e.g., understanding the amount of energy carried by the jet. New studies are being currently undertaken by several groups from both spectral and timing point of view, and much progress is expected in the forthcoming years in this relatively young field. Here, it is worthy to notice the timing capabilities of ASTROSAT in the UV, that could be exploited in the very near future.

8. Dynamical measurements of black hole masses

At present, more than ~ 20 of X-ray binaries where the compact object is heavier than $3M_{\odot}$ have been found, with masses as high as $\sim 15M_{\odot}$ (Orosz et al. 2007). Most of these measurements come from BHT, where the companion star is usually detectable during the quiescence epoch and classical techniques based on the Kepler laws (see e.g., Casares 2007 for a recent review) can be applied. However, this number is still not enough to have a good description of the mass spectrum of stellar mass BHs, and some open questions remain (e.g., is there a real gap in the distribution of masses of compact objects between NS and BHs?; see Özel et al. 2010). On the other hand, the mass is a key parameter for BH spin measurements (e.g., McClintock et al. 2011). New analysis methods (e.g., Hynes et al. 2003; Muñoz-Darias et al. 2008, Cantrell et al. 2010) and observing facilities (e.g., Corral-Santana et al. 2011) are allowing us to tackle faint systems and to infer more accurate masses. A big improvement will come with the next generation of telescopes (20–40 m), which will enable to study objects with very faint quiescence levels. Still, one of the main problems will be to discover more of those systems without the need that they go into outburst. This would increase significantly the number of dynamical mass measurements since the population of quiescence black holes is expected to be at least of the order of few thousands (see e.g., Romani 1998 and references therein).

9. Where do we go from here: ASTROSAT and LOFT

The natural successor of RXTE is the Indian multi-wavelength mission ASTROSAT (Agrawal 2006), which is currently schedule for launch by the second half of 2012. While its all-sky monitor (SSM) will allow good coverage of the transient X-ray sky and its UV telescope (UVIT) will observe the very few BHTs which are not affected by very high absorption, its X-ray pointed instruments will extend the RXTE characteristics and make it possible to continue and extend the study of bright BHT transients. The soft X-ray telescope (SXT: 0.3–8 keV) and the coded-mask imager (CZTI: 10–150 keV) will complement the large proportional counter array (LAXPC: 3–

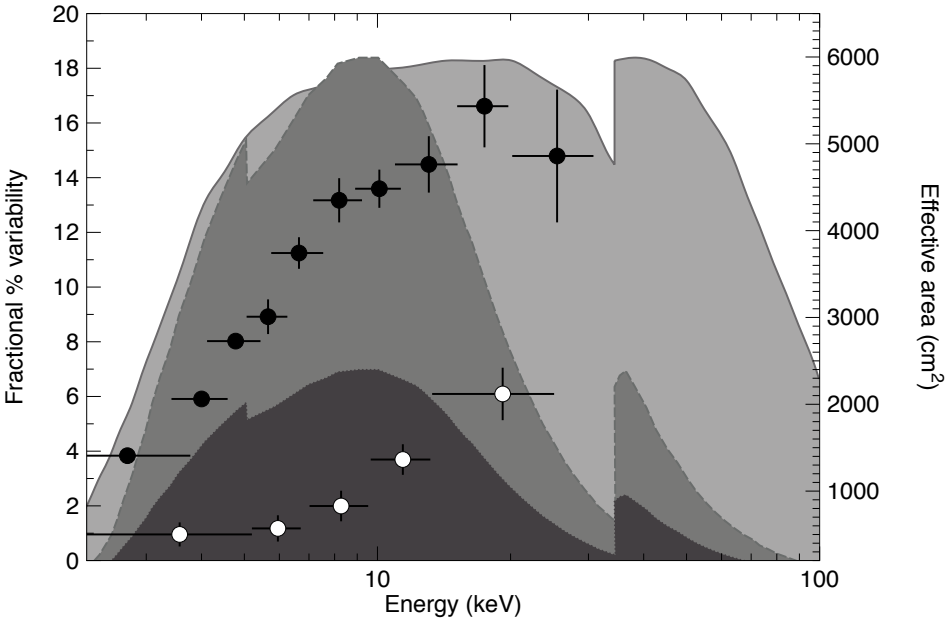

Figure 6. A comparison of instrument effective areas and energy-dependent variability for selected signals. Dark gray: area of RXTE/PCA (2 units); medium gray: RXTE/PCA effective area (5 units); light gray: ASTROSAT/LAXPC effective area (3 units). The black points report the energy dependent fractional rms variability of the type-C QPO in XTE J1859+226 (from Casella et al. 2004), the white points that of the HFQPO in GRS 1915+105 (from Morgan et al. 1997).

80 keV) to produce broad-band X-spectra, and the LAXPC effective area (6000 cm^2 at 10 keV) will yield the large photon counting necessary for fast-timing studies.

For the most distant future, not before 2020, the LOFT mission has been proposed and is being evaluated (Feroci et al. 2011). The effective area of the LAD instrument is currently being planned to be 12 m^2 at 8 keV, clearly a major step forward compared to current instrumentation. With LOFT, it will be possible to detect HFQPOs at very low fractional rms, therefore unveiling its nature by examining the distribution in detected frequencies (one of the current models predicts that the frequencies are constant), while the relative variation of the frequencies will tell us to which relativistic time scales, if any, they correspond to. Moreover, a very large collecting area will allow the detection of a sufficiently high number of photons to study low-frequency oscillations directly in the time domain, opening the possibility of understanding the nature of their quasi-periodicity and its connection to accretion and General Relativity. The good energy resolution will also make it possible to link fast variations to spectral measurements, tying two parallel aspects connected to relativistic effects, a subject that it is barely possible to touch with RXTE.

For the phenomenology described above, the LAXPC effective area is particularly interesting. While comparable to that of the RXTE/PCA below 10 keV, between 10 and 80 keV the LAXPC will be much more sensitive (in particular since later PCA observations are performed with 1 or 2 detector units, see Fig. 6). All timing signals from BHTs, with the exception of the strong noise in the LHS, are stronger at high energies. In Fig. 6 are shown the energy dependence of a type-C QPO and a HFQPO, superimposed on the PCA and LAXPC effective areas. It is clear that the higher sensitivity of the LAXPC above 10 keV will allow the study of weaker signals and in particular will offer the possibility to detect new HFQPOs in addition to the handful already available.

As the observational constraints of ASTROSAT will not be the same as those of RXTE, it is important to plan the best observational strategy for BHTs. An extremely dense coverage of outbursts such as that in Fig. 1 is most likely not going to be available, at least in the first phases of the mission. However, the detailed knowledge of the phenomenology described in the previous sections make it sure that even selected pointings, triggered by other instruments such as the SSM, MAXI, INTEGRAL/IBIS or Swift/BAT, have the potential of a late yield. In particular, a strategy of fewer longer observations in correspondence of main transition and states will generate crucial data, especially if coordinated with observations at lower wavelengths (radio, IR) from the ground.

Acknowledgements

SM and TB acknowledge support from grant ASI-INAF I/009/10/. The research leading to these results has received funding from PRIN INAF 2007 and from the European Community's Seventh Framework Programme (FP7/2007-2013) under grant agreement number ITN 215212 'Black Hole Universe'. Partially funded by the Spanish MEC under the Consolider-Ingenio 2010 Program grant CSD2006-00070: 'First Science with the GTC' (http://www.iac.es/consolider-ingenio-gtc/).

References

Agrawal P. C., 2006, AdSpR, 38, 2989
Belloni T. M., 2010, in Belloni T., ed, The jet paradigm: from microquasars to quasars, Lecture Notes in Physics, Springer Verlag, Berlin, 794, 53
Belloni T., Méndez M., Sánchez-Fernández C., 2001, A&A, 372, 551
Belloni T., Psaltis D., van der Klis M., 2002, ApJ, 572, 392
Belloni T., Homan J., Casella P., van der Klis M., Nespoli E., Lewin W. H. G., Miller J. M., Méndez M., 2005, A&A, 440, 207
Belloni T., Soleri P., Casella P., Méndez M., Migliari S., 2006, MNRAS, 369, 305
Brocksopp C., et al., 2002, MNRAS, 331, 765
Cantrell A. G., et al. 2010, ApJ, 710, 1127
Capitanio F., Belloni T., Del Santo M., Ubertini P., 2009, MNRAS, 398, 1194
Casares J., 2007, IAU Symposium, 238, 3

Casares J., Charles P. A., Naylor T., 1992, Nature, 355, 614
Casella P., Belloni T., Homan J., Stella L., 2004, A&A, 426, 587
Casella P., Belloni T., Stella L., 2005, ApJ, 629, 403
Casella P., et al., 2010, MNRAS, 404, L21
Coriat M., et al., 2011, MNRAS, 414, 677
Corral-Santana J. M., Casares J., Shahbaz T., Zurita C., Martínez-Pais I. G., Rodríguez-Gil P., 2011, MNRAS, 413, L15
Del Santo M., Malzac J., Jourdain E., Belloni T., Ubertini P., 2008, MNRAS, 390, 227
Dhillon V. S., et al., 2007, MNRAS, 378, 825
Done C., Kubota A., 2006, MNRAS, 371, 1216
Done C., Gierliński M., Kubota A., 2007, The Astronomy and Astrophysics Review, 15, 1
Dunn R. J. H., Fender R. P., Körding E. G., Belloni T., Cabanac C., 2010, MNRAS, 403, 61
Durant M., Gandhi P., Shahbaz T., Fabian A. P., Miller J., Dhillon V. S., Marsh, T. R., 2008, ApJ, 682, L45
Elvis M., Page C. G., Pounds K. A., Ricketts M. J., Turner M. J. L., 1975, Nature, 257, 656
Fender R., Belloni T., 2004, ARA&A, 42, 317
Fender R. P., Belloni T. M., Gallo E., 2004, MNRAS, 355, 1105
Fender R. P., Homan J., Belloni T. M., 2009, MNRAS, 396, 1370
Fender R., 2010, in Belloni T., ed, The jet paradigm: from microquasars to quasars, Lecture Notes in Physics, Springer Verlag, Berlin, 794, 115
Feroci, M., & LOFT Consortium, 2011, arXiv:1107.0436
Gallo E., 2010, in Belloni T., ed, The jet paradigm: from microquasars to quasars, Lecture Notes in Physics, Springer Verlag, Berlin, 794, 85
Gallo E., Fender R. P., Miller-Jones J. C. A., Merloni A., Jonker P. G., Heinz S., Maccarone T. J., van der Klis M., 2006, MNRAS, 370, 1351
Gierliński M., Zdziarski, A. A., 2005, MNRAS, 363, 1349
Gilfanov, M. 2010, in Belloni T., ed, The jet paradigm: from microquasars to quasars, Lecture Notes in Physics, Springer Verlag, Berlin, 794, 17
Gleissner T., Wilms J., Pottschmidt K., Uttley P., Nowak M. A., Staubert R., 2004, A&A, 414, 1091
Homan J., Wijnands R., van der Klis M., Belloni T., van Paradijs J., Klein-Wolt M., Fender R., Méndez M., 2001, ApJS, 132, 377
Homan J., Belloni T., 2005, Ap&SS, 300, 107
Homan J., Buxton M., Markoff S., Bailyn C. D., Nespoli E., Belloni T., 2005, ApJ, 624, 295
Hynes R. I., et al., 2003, MNRAS, 345, 292
Hynes R. I., Steeghs D., Casares J., Charles P. A., O'Brien, K., 2003, ApJ, 583, L95
Joinet A., Kalemci E., Senziani F., 2008, ApJ, 679, 655
Kalemci E., Tomsick J. A., Rothschild R. E., Pottschmidt K., Corbel S., Kaaret P., 2006, ApJ, 639, 340
Kanbach G., Straubmeier C., Spruit H. C., Belloni, T., 2001, Nature, 414, 180
Laurent P., Titarchuk L., 2001, ApJ, 562, L67
Maccarone T. J., Coppi P. S., 2003, MNRAS, 338, 189
Maccarone T. J., 2003, A&A, 409, 697
Maccarone T. J., Schnittman J. D., 2005, MNRAS, 357, 12

Malzac J., Merloni A., Fabian, A. C., 2004, MNRAS, 351, 253
Markoff S., 2010, in Belloni T., ed, The jet paradigm: from microquasars to quasars, Lecture Notes in Physics, Springer Verlag, Berlin, 794, 143
Markoff S., Falcke, H., Fender, R., 2001, A&A, 372, L25
Markoff S., Falcke H., Fender, R., 2002, APS Meeting Abstracts, 17105
McClintock J. E., Remillard, R. A., 1986, ApJ, 308, 110
McClintock J. E., et al., 2011, Classical and Quantum Gravity, 28, 114009
Migliari S., et al., 2007, ApJ, 670, 610
Miyamoto S., Kitamoto S., Iga S., Negoro H., Terada K., 1992, ApJ, 391, L21
Miyamoto S., Iga S., Kitamoto S., Kamado Y., 1993, ApJ, 403, L39
Morgan E. H., Remillard R. A., Greiner J., 1997, ApJ, 482, 993
Motta S., Belloni T., Homan, J., 2009, MNRAS, 400, 1603
Motta S., Muñoz-Darias T., Belloni T., 2010, MNRAS, 408, 1796
Motta S., Muñoz-Darias T., Casella P., Belloni T., Homan J., 2011, MNRAS, in press (arXiv:1108.0540)
Muñoz-Darias T., Martínez-Pais I. G., Casares J., Dhillon V. S., Marsh T. R., Cornelisse R., Steeghs D., Charles, P. A., 2007, MNRAS, 379, 1637
Muñoz-Darias T., Casares J., Martínez-Pais I. G., 2008, MNRAS, 385, 2205
Muñoz-Darias T., Motta S., Pawar D., Belloni T. M., Campana S., Bhattacharya, D., 2010, MNRAS, 404, L94
Muñoz-Darias T., Motta S., Belloni, T. M., 2011a, MNRAS, 410, 679
Muñoz-Darias T., Motta S., Stiele H., Belloni, T. M. 2011b, MNRAS, 415, 292
Nespoli E., Belloni T., Homan J., Miller J. M., Lewin W. H. G., Méndez M., van der Klis M., 2003, A&A, 412, 235
Nowak M. A., Vaughan B. A., 1996, MNRAS, 280, 227
Orosz J. A., et al., 2007, Nature, 449, 872
Özel F., Psaltis D., Narayan R., McClintock, J. E., 2010, ApJ, 725, 1918
Rao F., Belloni T., Stella L., Zhang S. N., Li T., 2010, ApJ, 714, 1065
Reig P., Belloni T., van der Klis M., 2003, A&A, 412, 229
Remillard R. A., McClintock J. E., 2006, ARA&A, 44, 49
Remillard R. A., Sobczak G. J., Muno M. P., McClintock J. E., 2002, ApJ, 564, 962
Romani R. W., 1998, A&A, 333, 583
Russell D. M., Fender R. P., Hynes R. I., Brocksopp C., Homan J., Jonker P. G., Buxton M. M., 2006, MNRAS, 371, 1334
Russell D. M., Maitra D., Dunn R. J. H., Markoff, S., 2010, MNRAS, 405, 1759
Russell D. M., Miller-Jones J. C. A., Maccarone T. J., Yang Y. J., Fender R. P., Lewis F., 2011, MNRAS, in press (arXiv:1106.0723)
Soleri P., Belloni T., Casella P., 2008, MNRAS, 383, 1089
Stiele H., Motta S., Muñoz-Darias T., Belloni T. M., 2011, MNRAS, in press (arXiv:1108.2198)
Takizawa M., et al., 1997, ApJ, 489, 272
Tanaka Y., Lewin W. H. G., 1995, in Eds. Lewin W.H.G., van Paradijs J., van den Heuvel E.P.J., eds, X-ray binaries, Cambridge Univ. Press, p. 126
Uttley P., Wilkinson T., Cassatella P., Wilms J., Pottschmidt K., Hanke M., Bock M., 2011, MNRAS, 414, L60

van der Klis M., 2006, in Lewin W., van der Klis M., eds., Compact stellar X-ray sources, Cambridge University Press, Cambridge, p. 39
Veledina A., Poutanen J., Vurm, I., 2011, ApJ, 737, L17
Wijnands R., van der Klis, M., 1999, ApJ, 514, 939
Wijnands R., Homan J., van der Klis M., 1999, ApJ, 526, L33
Wilkinson T., Uttley P., 2009, MNRAS, 397, 666
Yu W., Yan Z., 2009, ApJ, 701, 1940
Zdziarski A. A., Poutanen J., Paciesas W. S., Wen, L., 2002, ApJ, 578, 357